Form factors and transition charge densities for the quadrupole and hexadecupole electroexcitation of some $2p$-$1f$ shell nuclei

P. K. Raina*
Department of Physics, Indian Institute of Technology, Kanpur 208016, India

S. K. Sharma†
International Centre for Theoretical Physics, Trieste, Italy
(Received 4 September 1987)

A microscopic description of the recent data on the inelastic electron scattering form factors for the $0^+ \rightarrow 2^+$ as well as $0^+ \rightarrow 4^+$ transitions in some doubly even Ti, Cr, Fe, Ni, and Zn isotopes is attempted in terms of the projected Hartree-Fock-Bogoliubov wave functions resulting from realistic effective interactions operating in the $2p$-$1f$ shell. It turns out that the available form factor data out to about 2.5 fm^{-1} can be reproduced in most of the cases in a fairly satisfactory manner in terms of reasonable values of effective charges. It is seen that the empirical transition charge densities in Ni and Zn isotopes extracted from the form factor data via the Fourier-Bessel analysis play a decisive role vis-à-vis the choice of a model of core-polarization contributions.

I. INTRODUCTION

Inelastic electron scattering has proved to be an excellent method for exploring nuclear structure.[1,2] A measurement of the electroexcitation cross section permits one to obtain nuclear dynamical properties such as the transition charge and current densities involved in the transition. The calculation of these transition densities in terms of nuclear wave functions provides a sensitive test of the latter.

Recent inelastic electron scattering experiments have provided valuable data on the $0^+ \rightarrow 2^+$ as well as $0^+ \rightarrow 4^+$ transitions in a number of doubly even $2p$-$1f$ shell nuclei.[3-7] Within a measured momentum-transfer range up to 3 fm^{-1} the observed $C2$ form factors are characterized by two distinct maxima appearing at $q_{\rm eff} \sim 0.7$ and 1.6 fm^{-1}. The maxima of the $C4$ form factors occur at $q_{\rm eff} \sim 1.2$ and 2.2 fm^{-1}. The relative magnitude of the form factors at the two maxima is expected to provide a sensitive test of the nuclear microscopic models involved in the calculations.

We showed earlier[8] that the yrast wave functions projected from the Hartree-Fock-Bogoliubov (HFB) intrinsic states resulting from realistic effective interactions operating in the full $2p$-$1f$ shell provide a good description of the observed form factors for the $0^+ \rightarrow 2^+_{1,2}$ transitions in some Ti, Cr, and Fe isotopes (with $46 \leq A \leq 56$) in the first half of the shell. In this paper we show that a similar description of the yrast wave functions also permits a fairly satisfactory interpretation of the available data on the 2^+ form factors in some doubly even Ni and Zn isotopes (with $58 \leq A \leq 68$) in the second half of the $2p$-$1f$ shell. In this context we discuss, for the first time, the microscopic prescription of calculating the transition charge densities in terms of self-consistent HFB states. We also examine here the recent form factor data[5-7] involving the $0^+ \rightarrow 4^+$ transitions in some Ti, Cr, Fe, and Ni isotopes in the framework of the projected HFB method.

Recently, Mooy and Glaudemans[9] have calculated the form factors as well as the transition charge densities for the $(0^+ \rightarrow 2^+)$ transitions in the nuclei ^{58,60,62}Ni in terms of shell model wave functions[10] resulting from semiempirical effective interactions operating in the restricted valence spaces involving the

$$[(2p_{3/2}, 1f_{5/2}, 2p_{1/2})^n + (1f_{7/2})^{-1}(2p_{3/2}, 1f_{5/2}, 2p_{1/2})^{n+1}]$$

configurations. The calculations involved an independent variation of the effective charges for protons and neutrons so as to fit the $B(E2; 0^+ \rightarrow 2^+)$ values as well as the ratio of the form factor at the first and second maxima for each isotope. However, such a procedure yielded significantly *mass-dependent* effective charges; the values for the proton effective charge, e_π, turned out to be (2.60, 3.30, 1.85) for the nuclei ^{58,60,62}Ni, respectively.

The available data on the reduced $E2$ transition probabilities in the Zn isotopes suggests enhanced rotational collectivity in these isotopes compared to that in the Ni isotopes.[11,12] It is thus desirable to have an extended shell model description of these isotopes involving more than just one $(1f_{7/2})_\pi$ hole. In view of the near-intractability of such a description—the dimensionalities of the matrices involved in the earlier shell model calculations[9] with smaller numbers of valence particles are already above 1000—the available form factor data in doubly even Zn isotopes have not been analyzed in a microscopic framework thus far.

In the present work we show that the use of $J^\pi = 0^+, 2^+$ states projected from the HFB wave functions generated in the *full* $2p$-$1f$ space leads to a fairly satisfactory unified interpretation of the available $|F|^2(0^+ \rightarrow 2^+)$ in the nuclei ^{58,60,62}Ni and ^{64,66,68}Zn in terms of reasonable value of nearly *mass-independent* effective charges. This set of effective charges is also

shown to yield excellent quantitative agreement between the calculated and the observed values of the reduced $E2$ transition probabilities in these nuclei.

In recent years considerable attention has been devoted to the coordinate-space reconstruction of the transition charge densities associated with the electroexcitation of nuclear levels in the framework of the Fourier-Bessel method of Dreher *et al.*;[13] these analyses have been carried out by Heisenberg[3] for the Ni isotopes and by Neuhausen[4] for the Zn isotopes. The empirical transition densities acquire significance vis-à-vis the test of model wave functions since they contain structural information unaffected by the accuracy of the usual plane-wave Born approximation (PWBA) for large momentum transfers. We have calculated here the transition charge densities for various Ni and Zn isotopes in terms of the projected HFB wave functions. By combining the model space transition densities resulting from the self-consistent wave functions with each of the two existing models for the core-polarization transition density, we have attempted to examine whether the empirical values point towards a preferred choice.

We have also calculated here the $|F|^2(0^+\rightarrow 4^+)$ values in the nuclei ^{48,50}Ti, ^{50,52,54}Cr, ^{54}Fe, and ^{60}Ni with a view toward testing the efficacy of the projected HFB description vis-à-vis the recently measured data for the electroexcitation of 4^+ levels in these nuclei. The recent work of Mooy and Glaudemans[9] has revealed that a restricted shell model description of the $(0^+\rightarrow 4^+)$ form factors in the nuclei ^{52}Cr, ^{54}Fe, and ^{60}Ni requires highly-mass-dependent effective charges which are also drastically different from the set required for a reasonable quantitative agreement with the observed $(0^+\rightarrow 2^+)$ form factors in these nuclei; the values $[e_\pi(0^+\rightarrow 2^+), e_\pi(0^+\rightarrow 4^+)]$ required to optimize the fit to the observed data are [1.33, 2.06], [1.42, 1.76], and [3.33, 1.54] for the isotopes ^{52}Cr, ^{54}Fe, and ^{60}Ni, respectively. In this context we find that the HFB description for the $J^\pi=4^+$ states in the Ti, Cr, Fe, and Ni isotopes not only obviates the necessity of invoking significant mass dependence, it also permits a good quantitative discussion of the $(0^+\rightarrow 4^+)$ form factors in terms of effective charges quite close to those required for a comparable fit to the $(0^+\rightarrow 2^+)$ data in these nuclei.

In Sec. II we present some details of the calculational framework. In Sec. III we discuss the form factors and transition densities, as well as the $E2$ transition strengths associated with the $(0^+\rightarrow 2^+)$ transition in some doubly even Ni and Zn isotopes. We shall also discuss in this section the results of the calculation of the $|F|^2(0^+\rightarrow 4^+)$ values in some Ti, Cr, Fe, and Ni isotopes. Section IV contains some concluding remarks.

II. CALCULATIONAL FRAMEWORK

In the calculations presented here we have employed a slightly modified version[14] of the Kuo-Brown (KB) effective interaction[15] for the

$$(1f_{7/2}, 2p_{3/2}, 2p_{1/2}, 1f_{5/2})$$

valence space. This interaction was shown earlier to be quite satisfactory from the point of view of reproducing the $B(E2;0^+\rightarrow 2^+)$ systematics and yrast spectra,[16] as well as the inelastic electron scattering form factors[8] involving the 2_1^+ and 2_2^+ states in several Ti, Cr, and Fe isotopes. The single particle energies for the $2p$-$1f$ orbits are taken from the observed ^{41}Ca spectrum.

For calculating the $(0^+\rightarrow 2^+)$ as well as $(0^+\rightarrow 4^+)$ form factors in various $2p$-$1f$ shell nuclei, we have obtained the axially symmetric intrinsic states by following three different methods—the HFB method discussed in Ref. 17 for the nuclei ^{48}Ti, ^{50,54}Cr, and ^{58,60}Ni, the deformed Hartree-Fock–Bardeen-Cooper-Schrieffer (HF-BCS) method discussed by Goodman[18] for the nuclei ^{50}Ti, ^{52}Cr, ^{54}Fe, ^{62}Ni, and ^{64}Zn, and the usual deformed HF method for the nuclei ^{66,68}Zn. Pairing correlations between only the like particles are allowed in our HFB and HF-BCS calculations. The choice of the intrinsic state for a particular nucleus has been dictated by the following considerations. It is seen that the inclusion of pairing correlations (in the HFB framework) results in nearly spherical intrinsic states in nuclei with $N=28$, and with $N\geq 34$. This is related to the fact that the usual HFB method does not permit a treatment of the deformation and pairing degrees of freedom on the same footing because of the subshell closure at $N=28$ and the approaching shell closure at $N=40$; it tends to emphasize the latter degrees of freedom. The near-spherical HFB intrinsic states for $N=28$ and $N\geq 34$ nuclei yield vanishingly small ($<10\%$) amplitudes for yrast states with $J>2$. These HFB intrinsic states are inappropriate vis-à-vis the present calculation, which requires, as an essential prerequisite, a reasonably satisfactory description of the $J^\pi=0^+$, 2^+, and 4^+ states. The HF-BCS intrinsic states for the nuclei ^{50}Ti, ^{52}Cr, ^{54}Fe, ^{62}Ni, and ^{64}Zn, and the HF intrinsic states for the nuclei ^{66,68}Zn, contain $J=2,4$ states with sizable ($>10\%$) amplitudes.

The use of the projected HFB/HF-BCS wave functions in the context of the calculation of the transition densities has not been discussed so far in the literature. In what follows we briefly sketch an outline of the method.[19]

The axially symmetric intrinsic HFB (or HF-BCS) state with $K=\langle J_z\rangle=0$ can be written as

$$|\Phi_0\rangle=\prod_{im}(u_i^m+v_i^m b_{im}^\dagger b_{i\bar{m}}^\dagger)|0\rangle \tag{1}$$

when the creation operators $b_{im}^\dagger$ can be expressed as

$$b_{im}^\dagger=\sum_j c_{ji}^m a_{jm}^\dagger,\quad b_{i\bar{m}}^\dagger=\sum_j(-1)^{j-m}c_{ji}^m a_{jm}^\dagger\ . \tag{2}$$

Here the operator $a_{jm}^\dagger$ creates a particle in the orbit $|jm\rangle$, and c_{ji}^m are the expansion coefficients. The index j labels the single particle states $1f_{7/2}$, $2p_{3/2}$, $2p_{1/2}$, and $1f_{5/2}$, and the index i is employed to distinguish between different states with the same m.

The states with good angular momenta J projected from the HFB state $|\Phi_K\rangle$ can be written as

$$|JK\rangle=P_{KK}^J|\Phi_K\rangle$$
$$=[(2J+1)/8\pi^2]\int D_{KK}^J(\Omega)R(\Omega)|\Phi_K\rangle d\Omega\ , \tag{3}$$

where $R(\Omega)$ and $D^J_{KK}(\Omega)$ are the rotation operator and the rotation matrix, respectively.

The nuclear charge density operator can be expanded in multipoles:

$$\hat{\rho}(r)=\sum_{\lambda\mu}\hat{\rho}_{\lambda\mu}(r)Y_{\lambda\mu}(\theta,\phi)\ . \tag{4}$$

The transition charge density $\rho_\lambda(r)$ is the reduced matrix element of $\hat{\rho}_\lambda$:

$$\rho_\lambda(r)=\langle J_f\|\hat{\rho}_\lambda\|J_i\rangle\ . \tag{5}$$

Using the projected HFB wave functions given by Eq. (3), one obtains the following expression for the transition charge density:

$$\begin{aligned}\rho_\lambda(J_i\to J_f)&=\langle J_f0\,|\,\hat{\rho}_\lambda(r)\,|\,J_i0\rangle\\&=(n^{J_f}n^{J_i})^{-1/2}\sqrt{(2J_i+1)}\int_0^{\pi/2}\sum_\mu\begin{bmatrix}J_i&\lambda&J_f\\-\mu&\mu&0\end{bmatrix}d^{J_i}_{-\mu0}(\theta)n(\theta)\\&\quad\times\left[\sum_{k,\alpha,\beta}e_kR_{n_\alpha l_\alpha}(r)R_{n_\beta l_\beta}(r)\langle\alpha\,|\,Y^{(L)}_{M'}\,|\,\beta\rangle\left[\frac{M(\theta)}{1+M(\theta)}\right]_{\alpha\beta}\right]\sin\theta\,d\theta\ .\end{aligned} \tag{6}$$

Here the term in square brackets is a Clebsch-Gordan coefficient, and $R_{nl}(r)$ is the radial part of the harmonic oscillator states $|nl\rangle$. The functions $Y^{(L)}_M$ are the spherical harmonics of order L. The explicit expressions for the normalizations n^J and the matrices $n(\theta)$ and $M(\theta)$ are given in Ref. 8. The expressions for calculating the form factors and the reduced transition probabilities for electric quadrupole transitions, as well as the static quadrupole moments of the 2^+ states, have also been given in Ref. 8.

For the evaluation of the single particle matrix elements we have employed the oscillator wave functions with the length parameter given by $b=1.01A^{1/6}$. The center-of-mass correction[2] has been taken into account by multiplying a factor $\exp(b^2q^2/4A)$. The correction[6] due to the finite size of the proton has been incorporated by multiplying with the proton form factor $f_p(q)$:

$$f_p(q)=1/(1+q^2a_p^2/12)^2\ , \tag{7}$$

where $a_p=0.84$ fm.

Furthermore, in order to compare the form factors calculated by the PWBA with the experiments, the experimental data have been plotted at the effective momentum transfer $q_{\rm eff}$ instead of the kinematic q:

$$q_{\rm eff}=q\left[1+\frac{3Z\alpha\hbar c}{2E_iR_{\rm eq}}\right]\ , \tag{8}$$

where $R_{\rm eq}$ is the radius of the equivalent uniform charge distribution of the ground state and E_i is the energy of the incident electrons.

The recently measured[6] cross sections associated with the $0^+\to4^+$ transitions in the nuclei ^{50,52,54}Cr have been given as a function of the scattering angle. In these cases the momentum transfer q has been calculated using the relation

$$q=2(E_iE_f)^{1/2}\sin(\theta/2)\ , \tag{9}$$

where E_f denotes the final energy of the electron.

III. RESULTS AND DISCUSSION

A. The $0^+\to2^+$ transition in the nuclei ^{58,60,62}Ni and ^{64,66,68}Zn

1. Form factors

We first discuss here the Ni isotopes. The squared form factors $|F(q)|^2(0^+\to2^+)$ in these isotopes are calculated and compared with the experiments[3] in Fig. 1. The form factors have been computed with the effective charges $e_\pi=1.8$ for protons and $e_\nu=0.8$ for neutrons. As discussed later, it is seen that this set of effective charges is quite consistent with the available $B(E2;0^+\to2^+)$ values in these isotopes.

Overall, it is seen that the agreement between the calculated and the observed form factors is remarkably good throughout the momentum-transfer range $q=0.5$–2.8 fm^{-1}. The degree of quantitative agreement in the nuclei ^{58,60}Ni is quite satisfying, particularly in view of the fact that the effective charges were not fine tuned for each isotope.

A significant discrepancy occurs in the case of the nucleus ^{62}Ni where the present calculation underestimates the form factors for the range $q=0.8$–1.2 fm^{-1} by about 30 percent. This may be due to the noninclusion of the $1g_{9/2}$ orbit in the valence space. As pointed out by Delphini and Glaudemans,[20] as well as Potbhare *et al.*,[21] the $1g_{9/2}$ orbit is expected to play an important role vis-à-vis the structure of the yrast levels in Ni isotopes with $A\geq60$. However, the nonavailability of the core-renormalized effective interactions for the

$$(1f_{7/2},\,2p_{3/2},\,2p_{1/2},\,1f_{5/2},\,1g_{9/2})$$

space has prevented us from examining here the explicit role of the $1g_{9/2}$ orbit.

We have also presented in Fig. 1 the results obtained by Mooy and Glaudemans[9] in the framework of the shell model involving the

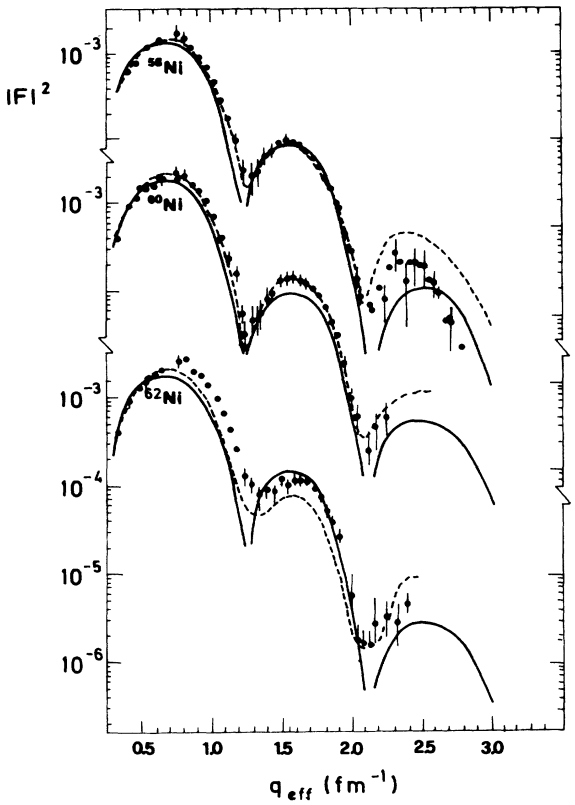

FIG. 1. Experimental and calculated squared form factors $|F|^2$ for the $0^+ \rightarrow 2^+$ transitions in the nuclei ^{58,60,62}Ni. The solid curves show the results obtained with the self-consistent wave functions. The broken curves display the results obtained in the recent shell model calculation (Ref. 9) involving restricted configuration mixing.

$$[(2p_{3/2}, 2p_{1/2}, 1f_{5/2})^n + (1f_{7/2})^{-1}(2p_{3/2}, 2p_{1/2}, 1f_{5/2})^{n+1}]$$

configurations. These calculations employed the effective charges $(e_\pi, e_\nu)=(2.60, 0.72)$, $(3.30, 0.50)$, and $(1.85, 0.82)$ for the nuclei ^{58,60,62}Ni, respectively.

Considering first the momentum-transfer range $0.5 < q < 2.1$ fm^{-1}, we find that the projected HFB and the shell model estimates are quite close except around the second maximum ($q \sim 1.6$ fm^{-1}) in the nucleus ^{62}Ni, where the latter are smaller by roughly a factor of 2. For larger momentum transfers the shell model estimates are an order of magnitude larger—a feature that emphasizes the desirability of precise form factor data for $q > 2.1$ fm^{-1} in the nuclei ^{60,62}Ni.

It is interesting to note that the proton effective charges employed in the shell model calculations in the nuclei ^{58,60}Ni are considerably larger than the A-independent value ($e_\pi = 1.8$) employed in the present work. This can be qualitatively understood in the following manner. The shell model value of the proton effective charge simulates partly the effects due to the excitations involving two or more $1f_{7/2}$ protons. Since the proton-neutron interactions are strongest for orbits with large spatial overlap, such processes are expected to be favored in the nuclei ^{58,60}Ni where the energy difference between the proton and neutron Fermi surfaces is not very large.[22] In heavier nuclei ($A \geq 62$) with larger neutron excess, the amplitude of proton excitations leading to correlated proton-neutron configurations is expected to decrease due to larger gap between the proton and neutron Fermi surfaces.

Figure 2 presents a comparison of the calculated and the experimental[4] $|F(q)|^2$ values for the $0^+ \rightarrow 2^+$ transitions in the nuclei ^{64,66,68}Zn. These form factors were analyzed earlier with phenomenological models—the modified Tassie model[23] and the Gaussian model.[2] The best-fit calculations carried out in the framework of the latter model have also been shown here.

As in the case of the Ni isotopes, the present form factor calculations for the Zn isotopes also employ effective charges such that the isovector effective charge, defined by $(e_\pi - e_\nu)$, is always $1e$. However, it turns out that a reasonable variation of the isoscalar effective charge—with $e_\nu = (0.75, 0.55, 0.75)$ for the nuclei ^{64,66,68}Zn, respectively—is required for optimizing the agreement with the available $B(E2; 0^+ \rightarrow 2^+)$ values. With these effective charges, the form factors for $q < 1.2$ fm^{-1} computed with the self-consistent wave functions are also in excellent agreement with the experiments.[4] We notice, however, systematic discrepancies between the calculat-

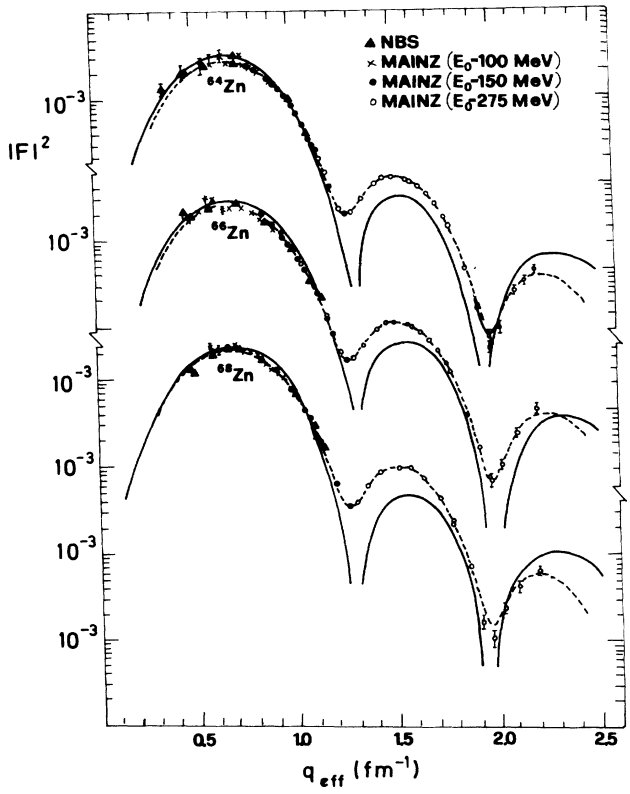

FIG. 2. Experimental and calculated form factors for the $0^+ \rightarrow 2^+$ transitions in the nuclei ^{64,66,68}Zn. The broken curves represent the best-fit calculations with the Fourier-Bessel expansion of the transition charge densities (Ref. 4).

TABLE I. The $Q(2^+)$ and $B(E2;0^+\rightarrow 2^+)$ values (labeled PHFB) in the nuclei ^{58,60,62}Ni and ^{64,66,68}Zn calculated with the set of effective charges employed in the form factor calculations. The $B(E2;0^+\rightarrow 2^+)$ values are in units of e^2fm^4 and the $Q(2^+)$ values have been given in units of e fm^2. Here, $\langle Q_0^2\rangle_\pi$ ($\langle Q_0^2\rangle_\nu$) gives the contribution of the valence protons (neutrons) to the intrinsic state.

Nucleus	$\langle Q_0^2\rangle$ $[\langle Q_0^2\rangle_\pi, \langle Q_0^2\rangle_\nu]$	(e_π, e_ν)	$B(E2;0^+\rightarrow 2^+)$ PHFB	$B(E2;0^+\rightarrow 2^+)$ Expt.	$Q(2^+)$ PHFB	$Q(2^+)$ Expt.
^{58}Ni	-3.4 $[-1.1, -2.3]$	(1.80, 0.80)	647	668±70[a]	2.8	−15±8[c]
^{60}Ni	-12.5 $[-3.9, -8.6]$	(1.80, 0.80)	846	909±70[a]	16.1	3±7[c]
^{62}Ni	-13.1 $[-5.3, -7.8]$	(1.80, 0.80)	970	876±75[a]	21.3	5±12[c]
^{64}Zn	-20.3 $[-10.1, -10.2]$	(1.75, 0.75)	1610	1580±50[b]	31.8	
^{66}Zn	-24.6 $[-13.5, -11.1]$	(1.55, 0.55)	1457	1370±50[b]	34.3	
^{68}Zn	-18.2 $[-9.8, -8.4]$	(1.75, 0.75)	1210	1360±60[b]	29.9	

[a]Reference 11.
[b]Reference 12.
[c]Reference 24.

ed and observed form factors for $q > 1.2$ fm^{-1}. The calculated form factors for $q \sim 1.5$ fm^{-1} are smaller by about 40 percent than the observed ones, and the second maxima of the theoretical form factors display a small but noticeable shift towards higher momentum transfer. These discrepancies may again be reflecting the necessity of explicit involvment of ^{40}Ca core excitations as well as the $1g_{9/2}$ excited configurations. Present calculations reveal (see the second column of Table I) that the total intrinsic quadrupole momenta for the Zn isotopes are substantially larger than those obtained for the lighter Ni isotopes. This onset of sizable oblate deformation may signal enhanced $1g_{9/2}$ occupation via a lowering of the (down sloping) Nilsson orbitals with $k = \pm\frac{9}{2}$.

As discussed later, the apparent inadequecy of the effective charges to simulate the excitations from the core into model space—or out of model space into higher orbits—in the context of large *momentum-transfer* data manifests itself in the form of discrepancies between the calculated and empirical transition densities in the interior region ($r < 3$ fm).

2. *The reduced transition probabilities, $B(E2;0^+\rightarrow 2^+)$, and the static quadrupole moments, $Q(2^+)$*

In Table I and Fig. 3 we have presented the results for the static quadrupole moments, $Q(2^+)$, as well as the reduced transition probabilities, $B(E2;0^+\rightarrow 2^+)$ in the nuclei ^{58,60,62}Ni and ^{64,66,68}Zn. The $Q(2^+)$ and $B(E2)$ values have been computed with the effective charges employed in the calculation of the form factors for various isotopes discussed in the preceding section. The calculated $B(E2;0^+\rightarrow 2^+)$ values are seen to be in excellent agreement with the experiments;[24] the only noticeable discrepancy occurs in the case of the nucleus ^{68}Zn where the present calculation underestimates the lower bound of the observed value by about 6.6 percent.

The usefulness of the available $Q(2^+)$ values—and these are just three in number—vis-à-vis a test of the present microscopic description is severely constrained by the large error bars arising due to the uncertainties

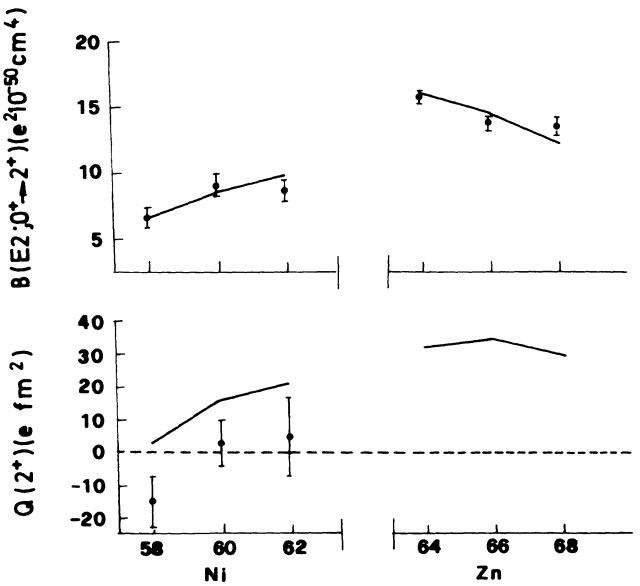

FIG. 3. Graphical presentation of the results for electric quadrupole transition probabilities and static quadrupole moments in some doubly even Ni and Zn isotopes. The straight lines join the points calculated with the effective charges employed in the form factor calculations.

associated with the effects of higher excited states in the Coulomb excitation processes. The calculated values are, however, qualitatively consistent with the available data; in particular, the latter seem to support our prediction of *oblate* intrinsic shapes in the nuclei ^{60,62}Ni.

3. *Transition charge densities*

In the preceding sections we have seen that the introduction of the state-independent—and (nearly) mass-independent—effective charges for the valence particles is, on the whole, quite adequate in most of the cases for describing the observed $B(E2)$ values and the form factors. The effective charge model implicitly assumes that the contributions arising from the core polarizations or the extra-model-space components are proportional to the valence space contributions. A more realistic model involves the mixing of the zeroth-order valence wave function with the 2^L pole, $n\hbar\omega$ giant resonances; this description is consistent with the use of the separable, multipole-multipole interaction in conjunction with the first-order perturbation theory. In view of the expected sensitivity of the transition densities towards the details of the radial characteristics of various parts of wave functions, we have also considered here this prescription for invoking core polarization by assuming the Tassie model[23] for the 2^L-pole excitations. The total transition density is constructed as the sum of two terms—the valence-space term $A(r)$ with isoscalar effective charge set to zero, and the Tassie core-polarization transition density term $B(r)$ (Ref. 25):

$$\rho(r)=A(r)+NB(r) , \tag{10}$$

when $B(r)$ is related to the ground state charge densities $\rho_{\text{g.s.}}(r)$ by the relation[4,9]

$$B(r)=r^{L-1}\frac{d}{dr}\rho_{\text{g.s.}}(r) . \tag{11}$$

The normalization constant N is obtained by requiring overall consistency with the usual effective charge model; we adjust N so that the total charge resulting from an integration of $\rho(r)$ is just e_π.

In Fig. 3 we present the transition charge densities for Ni isotopes calculated by combining the projected HFB predictions with one or the other of the two models for the core-polarization component. We have compared our results with the empirical transition densities extracted from the available form factor data in the framework of the Fourier-Bessel method by Heisenberg.[3] It is seen that in the region $3<r<8$ fm the predictions of the effective charge (dot-dashed line) and the Tassie prescriptions (dashed line) do not differ significantly. Whereas the latter prescription yields transition densities in excellent agreement with the empirical ones, the estimates involving the A-independent effective charges display minor discrepancies in ^{60,62}Ni. In the interior region ($0<r<3$ fm), however, the Tassie model for core polarization provides a vastly improved description of the transition densities, in keen contrast with the effective charge model estimates which show large oscillations. The effective charge model emphasizes the role of the underlying valence orbits. On the other hand, the collective contributions inherent in the Tassie model reduce considerably the single-particle features of the valence part.

We have also displayed in Fig. 4 the shell model results for transition densities obtained by Mooy and Glaudemans[9] with the effective charge prescription for the core polarization. The results are in qualitative agreement with the projected HFB estimates involving the effective charges. The quantitative differences arise from the enhanced $(1f_{7/2}\rightarrow 1f_{5/2})^\nu$ and $(1f_{7/2}\rightarrow 2p_{3/2})^\pi$ transitions allowed in the present calculations. As pointed out by Mooy and Glaudemans,[9] these transitions govern to a large extent the first maximum at $r\sim 1$ fm and the first minimum at $r\sim 2.5$ fm in the valence part of the transition densities.

In Fig. 5 we have presented a comparison of the projected HFB results for the transition densities in the nuclei ^{64,66,68}Zn with the empirical values extracted from

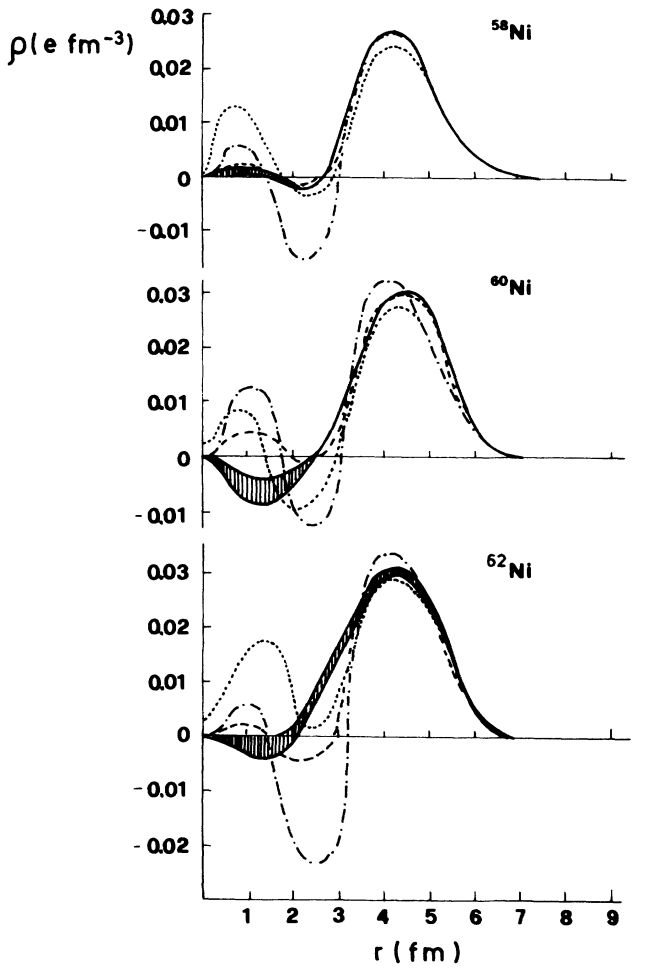

FIG. 4. Transition charge densities for the first 2^+ state in ^{58,60,62}Ni calculated with the effective charge model (dot-dashed line) and with the Tassie model (dashed line). The empirical charge densities (Ref. 3) have been shown in the form of an error band. The dotted curve represents the shell model results (Ref. 9).

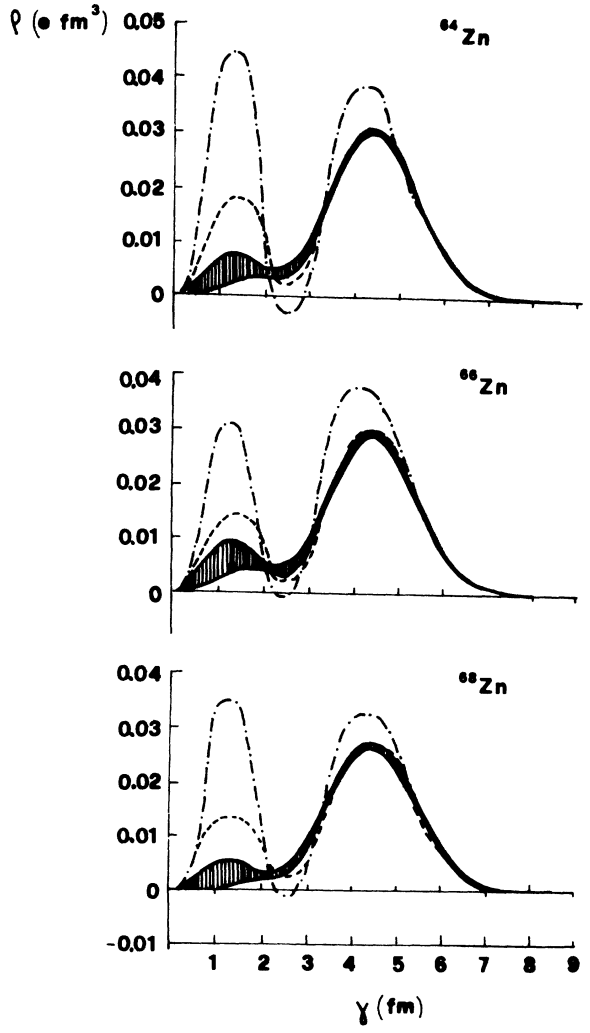

FIG. 5. The empirical transition densities (error band) and the theoretical predictions involving the effective charge model (dot-dashed lines) as well as the Tassie model (dotted lines).

the form factor data by Neuhausen.[4] Here again we find that the Tassie prescription for the core participation permits a significantly improved description of the empirical transition densities.

B. The $0^+ \rightarrow 4^+$ transition in the nuclei ^{48,50}Ti, ^{50,52,54}Fe, and ^{60}Ni

1. Qualitative features

The qualitative aspects of the $0^+ \rightarrow 4^+$ form factors in the $2p$-$1f$ shell nuclei are mainly governed by the two radial matrix elements $\langle 1f \mid j_4(qr) \mid 1f \rangle$ and $\langle 1f \mid j_4(qr) \mid 2p \rangle$, if we assume that the q dependence of these matrix elements is not significantly changed by the ^{40}Ca core-polarization processes. It turns out that (see Fig. 6) whereas the matrix element $\langle 1f \mid j_4(qr) \mid 1f \rangle$ possesses just one maximum at $q \sim 1.2$ fm^{-1}, the matrix element $\langle 1f \mid j_4(qr) \mid 2p \rangle$ possesses a maximum at $q \sim 1.1$ fm^{-1} followed by a minimum at $q \sim 2.2$ fm^{-1}. The zeros of the matrix elements $\langle 1f \mid j_4(qr) \mid 2p \rangle$ and

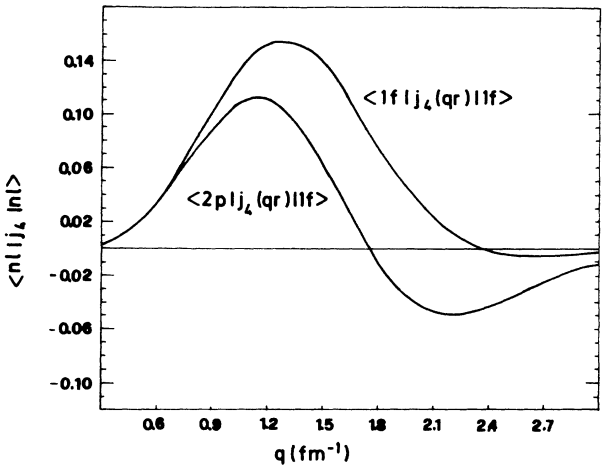

FIG. 6. The momentum-transfer dependence of the matrix elements $\langle nl \mid j_4(qr) \mid n'l' \rangle$ in the $2p$-$1f$ shell.

$\langle 1f \mid j_4(qr) \mid 1f \rangle$ occur at $q \sim 1.8$ and 2.4 fm^{-1}, respectively. Since the description of $F(q)$ in the projected HFB framework involves [see Eq. (8) in Ref. 8] a linear combination of the matrix elements $\langle 1f \mid j_4(qr) \mid 1f \rangle$ and $\langle 1f \mid j_4(qr) \mid 2p \rangle$, it is expected to display the following general features.

(i) In view of the proximity of the maxima of the two matrix elements, we do not expect significant A dependence in the position of the first maximum. This feature is strikingly reflected in the observed data;[5-7] the first maximum appears at practically the same position—at $q \sim 1.2$ fm^{-1}—in various nuclei.

(ii) We do not anticipate the occurrence of the second maximum in nuclei with structure dominated by the $(1f_{7/2})^n$ configurations for protons as well as neutrons, since in such cases the form factor is governed by only the matrix element $\langle 1f \mid j_4(qr) \mid 1f \rangle$.

(iii) In the deformed $2p$-$1f$ shell nuclei, the $2p_{3/2}$ orbit is also expected to play an important role. The magnitude of $|F(q)|^2$ at the second maximum as well as the location of this maximum is, therefore, expected to display considerable variation over the range $q = 1.8$ -2.5 fm^{-1}, depending on the relative importance of the matrix element $\langle 1f \mid j_4(qr) \mid 2p \rangle$.

2. The nuclei with N or Z=28

The squared form factors for the $0^+ \rightarrow 4^+$ transitions in the nuclei ^{50}Ti, ^{52}Cr, ^{54}Fe, and ^{60}Ni are calculated and compared with the experiments[5-7] in Fig. 7. In the calculations reported in this and the next subsection, we have employed the mass-independent set of effective charges $(e_\pi, e_\nu) = (1.5, 0.5)$ for the nuclei ^{48,50}Ti and ^{50,52,54}Cr. In the case of the nuclei ^{54}Fe and ^{60}Ni, the values employed are (1.7, 0.7) and (1.8, 0.8), respectively.

From the results presented in Fig. 7 one finds that the calculated form factors are in very good quantitative agreement with the experiments.[6] In the case of the nucleus ^{52}Cr present calculation correctly predicts the position as well as the magnitude of the second maximum.

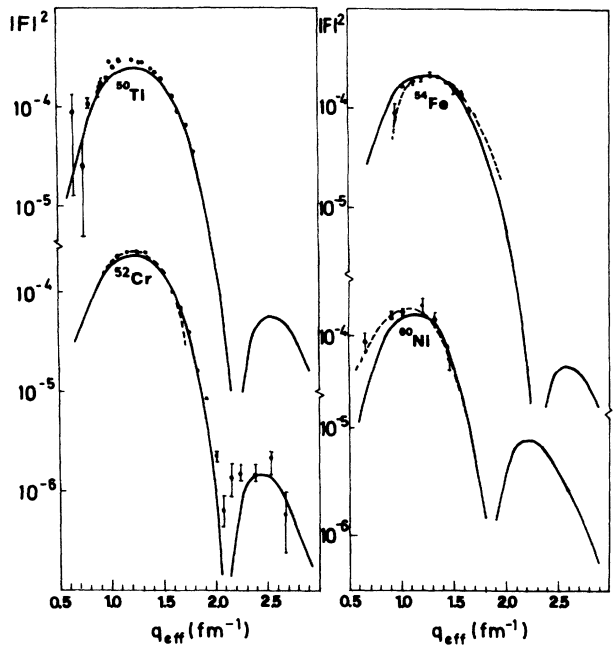

FIG. 7. Experimental and calculated squared form factors $|F|^2$ for the $0^+ \rightarrow 4^+$ transition in the nuclei ^{50}Ti, ^{52}Cr, ^{54}Fe, and ^{60}Ni. The broken curves show the shell model results (Ref. 9).

It is seen that a lack of enough reliable data points for $q < 1.0$ fm^{-1} prevents a detailed test of the calculated results. The importance of the low-q data for the $0^+ \rightarrow 4^+$ transitions is further emphasized by the fact that the experimental values for $B(4; 0^+ \rightarrow 4^+)$—and these are the limits of the relevant form factors as q approaches zero—are not available for testing the microscopic description. This contrasts keenly with the situation in the case of the $0^+ \rightarrow 2^+$ transition; in this case the $|F(q)|^2$ estimates for $q < 1$ are usually supplemented by the $B(E2)$ values deduced from the measured 2^+ half-lives.

We find that in the nuclei considered here the magnitude of the calculated $|F(q)|^2$ at the second maximum is smaller by more than 2 orders of magnitude compared to the values at the first maximum. In view of the general discussion of the form factors given earlier, the result implies the dominance of the $(1f_{7/2})^n$ configurations in the yrast states with $J^\pi = 0^+, 4^+$ in these nuclei.

We have also given in Fig. 7 the results obtained by Mooy and Glaudemans[9] in the case of the nuclei ^{52}Cr, ^{54}Fe, and ^{60}Ni. The effective charges $(e_\pi, e_\nu) = (2.06, 1.06)$, $(1.76, 0.76)$, and $(1.54, 0.54)$ were employed for the nuclei ^{50}Cr, ^{54}Fe, and ^{60}Ni, respectively, in the calculations. The shell model calculations have been reported only for the range $q = 0.6$–1.8 fm^{-1} covering just the first maxima; the calculations reproduce the observed data quite well in this momentum-transfer range. We note that in the nucleus ^{52}Cr, the shell model

TABLE II. The $B(E2; 0^+ \rightarrow 2^+)$ and $B(E4; 0^+ \rightarrow 4^+)$ values in the nuclei ^{48,50}Ti, ^{50,52,54}Cr, ^{54}Fe, and ^{60}Ni. The $B(E4)$ values have been calculated with the set of effective charges employed for calculating the form factors for the $0^+ \rightarrow 4^+$ transition. The $B(EL; 0^+ \rightarrow L^+)$ values are in units of $e^2\text{fm}^{2L}$. Here, $\langle Q_0^L \rangle_\pi$ ($\langle Q_0^L \rangle_\nu$) gives the contribution of the valence protons (neutrons) towards the 2^L-pole moment of the intrinsic state. The reduced transition probabilities resulting from the present calculation have been compared with the predictions of the recent shell model calculations (Ref. 9) (labeled SM) in some cases.

			$B(E2; 0^+ \rightarrow 2^+)$			$B(E4; 0^+ \rightarrow 4^+)$	
Nucleus	$\langle Q_0^2 \rangle$ $[\langle Q_0^2 \rangle_\pi, \langle Q_0^2 \rangle_\nu]$	$\langle Q_0^4 \rangle$ $[\langle Q_0^4 \rangle_\pi, \langle Q_0^4 \rangle_\nu]$	PHFB $[e_\pi, e_\nu]$	SM[a] $[e_\pi, e_\nu]$	Expt.[b]	PHFB $[e_\pi, e_\nu]$	SM[a] $[e_\pi, e_\nu]$
^{48}Ti	16.4	21.3	547		690±40	1.61×10^3	
	[6.7, 9.7]	[16.5, 4.8]	[1.7, 0.7]		750±50	[1.5, 0.5]	
^{50}Ti	−9.4	14.9	378		330±40	2.36×10^3	
	[−4.8, −4.6]	[6.1, 8.8]	[1.7, 0.7]		315±30	[1.5, 0.5]	
^{50}Cr	26.3	33.2	1302		1040±115	1.23×10^3	
	[13.0, 13.3]	[19.1, 14.1]	[1.6, 0.6]		1135±100	[1.5, 0.5]	
^{52}Cr	11.4	15.7	727	635	565±50	2.65×10^3	7.9×10^4
	[7.8, 3.6]	[9.7, 6.0]	[1.7, 0.7]	[1.3, 1.6]	660±30	[1.5, 0.5]	[2.06, 1.06]
^{54}Cr	26.7	33.7	1232		1000±70[c]	2.33×10^3	
	[13.1, 13.6]	[20.3, 13.4]	[1.5, 0.5]			[1.5, 0.5]	
^{54}Fe	9.0	−7.5	600	500	535±40[d]	2.91×10^3	1.3×10^5
	[6.4, 2.6]	[−5.5, −2.0]	[1.7, 0.7]	[1.4, 2.3]	675±40	[1.7, 0.7]	[1.76, 0.76]
^{60}Ni	−12.5	17.3	846	909	914±20[c]	3.46×10^3	2.2×10^5
	[−3.9, −8.6]	[9.1, 8.2]	[1.8, 0.8]	[3.3, 0.5]		[1.8, 0.8]	[1.54, 0.54]

[a]Reference 9.
[b]Reference 26.
[c]Reference 24.
[d]Reference 27.

(e_π, e_ν) values are considerably larger than those considered in the present calculation. Large renormalized values of the effective charge, which imply an enhanced involvement of the $2p_{3/2}$ orbit, are not unexpected in this nucleus in view of the significant nonsphericity of the zeroth-order description of the proton wave function in terms of the $(1f_{7/2})^{4\pi}$ configuration.

It may be pointed out here that the effective charges employed in the present calculation of the $0^+ \rightarrow 4^+$ form factor for various $2p$-$1f$ shell nuclei are either the same or lie within 12 percent of the values employed in our earlier calculations[8] for the $0^+ \rightarrow 2^+$ form factors in these nuclei. This feature is not shared by the shell model calculations (see columns 5 and 7, Table II); the shell model results are characterized by large differences between the effective charges employed for the $0^+ \rightarrow 2^+$ transitions and those for the $0^+ \rightarrow 4^+$ transition.

3. *The nuclei ^{48}Ti, ^{50}Cr, and ^{54}Cr*

Figure 8 compares the calculated and observed $|F|^2$ for the $0^+ \rightarrow 4^+$ transitions in the nuclei ^{48}Ti, ^{50}Cr, and ^{54}Cr.

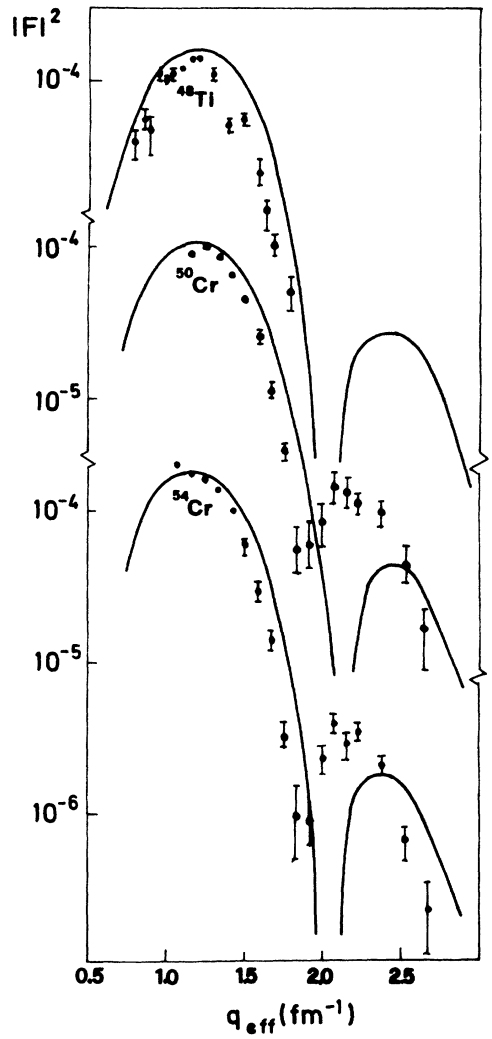

FIG. 8. Experimental and calculated squared form factors $|F|^2$ for the $0^+ \rightarrow 4^+$ transition in the nuclei ^{48}Ti, ^{50}Cr, and ^{54}Cr.

Although the $0^+ \rightarrow 2^+$ transitions in the nuclei ^{48}Ti and ^{50}Cr have been discussed earlier by Iwamoto *et al.*[28] in the framework of the shell model involving restricted configurations, no shell model calculation has so far been reported in these nuclei for the $0^+ \rightarrow 4^+$ form factors. Since these nuclei do not involve the $1f_{7/2}$ subshell closure, it is difficult to justify *a priori* any truncation scheme for reducing the number of shell model configurations.

As mentioned earlier, the projected HFB calculations have been carried out with a constant set of effective charges—with $e_\pi = 1.5$ and $e_\nu = 0.5$—for the nuclei considered here. It is seen that the present calculation is quite successful in reproducing the magnitude of the form factors at the first maxima. However, one observes discrepancies in the momentum-transfer range $1.5 < q < 2.7$ fm^{-1}; the position of the first minimum is shifted towards higher momentum transfers and the calculation underestimates the magnitude of $|F|^2$ around its second maximum in the nuclei ^{50,54}Cr. It is seen that the quadrupole moments of the intrinsic states (see column 2, Table II) in the nuclei ^{48}Ti and ^{50,54}Cr are significantly larger than those for the nuclei with N or $Z = 28$. The onset of sizable quadrupole deformations may warrant the inclusion of the $1g_{9/2}$ orbit in the configuration space. It would also be worthwhile to examine the effect of incorporating more configurational admixtures within the $2p$-$1f$ shell by considering quasiparticle-excited $K = 0$ intrinsic states, in addition to the usual one resulting from the HFB calculation.

IV. CONCLUSIONS

We have discussed here the calculation of the form factors associated with the electroexcitation of the 2^+ and 4^+ levels in a number of $2p$-$1f$ shell nuclei. The $BE(2)$ values as well as the transition charge densities have also been calculated in the case of the $0^+ \rightarrow 2^+$ transitions. It turns out that the projected HFB ansatz for the wave functions in conjunction with the realistic $2p$-$1f$ shell effective interactions provides a nearly parameter-free framework for interpreting and correlating the available data from a microscopic perspective.

Present calculations have revealed significant discrepancies vis-à-vis the large-momentum-transfer ($q > 2.0$ fm^{-1}) form factor data—and the related transition densities data for the interior region ($r > 3$)—in some cases. An explicit inclusion of the ^{40}Ca core excitations as well as $(1g_{9/2})^n$ configurations may lead to an improved description of the form factors and the transition densities, apart from reducing considerably the quantitative significance of the choice of a model for "effective charge" contributions.

One of the authors (S.K.S.) would like to thank Professor Abdus Salam, the International Atomic Energy Agency, and UNESCO for hospitality at the International Centre for Theoretical Physics, Trieste.

*Permanent address: Department of Physics, Himachal Pradesh University, Simla 171005, India.
†Permanent address: Department of Physics, Indian Institute of Technology, Kanpur 208016, India.

[1]T. de Forest and J. D. Walecka, Adv. Phys. **15**, 1 (1966).
[2]H. Überall, *Electron Scattering from Complex Nuclei* (Academic, New York, 1971).
[3]J. Heisenberg, in *Advances in Nuclear Physics,* edited by J. W. Negele and E. Vogt (Plenum, New York, 1981), Vol. 12.
[4]R. Neuhausen, Nucl. Phys. **A282**, 125 (1977).
[5]K. Hayakawa *et al.*, Res. Rep. Nucl. Sc. (Tohoku Univ.) **11**, 1 (1978).
[6]J. W. Lightbody, Jr. *et al.*, Phys. Rev. C **27**, 113 (1983).
[7]Y. Torizuka *et al.*, Phys. Rev. **185**, 1499 (1969).
[8]G. Mukherjee and S. K. Sharma, Phys. Rev. C **29**, 2101 (1984); **31**, 689 (1985).
[9]R. B. M. Mooy and P. W. M. Glaudemans, Nucl. Phys. **A438**, 461 (1985).
[10]R. B. M. Mooy and P. W. M. Glaudemans, Z. Phys. A **312**, 59 (1983).
[11]P. M. Endt, At. Nucl. Data Tables **23**, 547 (1979).
[12]J. F. Bruandet *et al.*, in *Proceedings of the EPS International Conference,* Florence (Italy), 1977, edited by P. Blasi and R. A. Ricci (Editrice Compositori, Bologna, 1978), p. 535.
[13]B. Dreher *et al.*, Nucl. Phys. **A235**, 219 (1974); H. Rothaas, J. Friedrich, K. Merle, and B. Dreher, Phys. Lett. **51B**, 23 (1974).
[14]J. B. McGrory, B. H. Wildenthal, and E. C. Halbert, Phys. Rev. C **2**, 186 (1970).
[15]T. T. S. Kuo and G. E. Brown, Nucl. Phys. **A114**, 241 (1968).
[16]S. K. Sharma, Nucl. Phys. **A260**, 226 (1976).
[17]C. Bloch and A. Messiah, Nucl. Phys. **39**, 95 (1962); S. B. Khadkikar and M. R. Gunye, *ibid.* **A144**, 289 (1970).
[18]A. L. Goodman, in *Advances in Nuclear Physics,* edited by J. W. Negele and E. Vogt (Plenum, New York, 1979), Vol. 11.
[19]N. Onishi and S. Yoshida, Nucl. Phys. **80**, 367 (1966).
[20]M. G. Delphini and P. W. M. Glaudemans, Z. Phys. A **317**, 357 (1984).
[21]V. Potbhare, S. K. Sharma, and S. P. Pandya, Phys. Rev. C **24**, 2355 (1981).
[22]B. Ghosh and S. K. Sharma, Phys. Rev. C **29**, 648 (1984).
[23]L. J. Tassie, Aust. J. Phys. **9**, 407 (1956).
[24]A. Christy and O. Häusser, Nucl. Data Tables **11**, 281 (1972).
[25]B. A. Brown, R. Radhi, and B. H. Wildenthal, Phys. Rep. **101**, 313 (1983).
[26]W. Kutschera, in *Proceedings of the EPS International Conference,* Florence (Italy), 1977, edited by P. Blasi and R. A. Ricci (Editrice Compositori, Bologna, 1978), p. 120.
[27]M. J. Levine, E. K. Warburton, and D. Schwalm, Phys. Rev. C **23**, 244 (1981).
[28]T. Iwamoto, H. Horie, and A. Yokoyama, Phys. Rev. C **25**, 658 (1982).